ENGINEERING Information Technology & Electronic Engineering
https://www.academax.com/EITEE; https://www.engineering.org.cn
https://ieeexplore.ieee.org/xpl/RecentIssue.jsp?punumber=11344065
E-mail: eng.itee@zju.edu.cn

Engineering Journals

Available on IEEE Xplore®

Research Article
https://doi.org/10.1631/ENG.ITEE.2025.0065

Development and iterative learning-enhanced sliding mode control of a bioinspired knee exoskeleton

Yi LONG[1,2✉], Ning CHEN[3], Zhibin CAI[4], Hexiao GUO[4], Yutian CHI[5], Wei DONG[5]

[1]*Faculty of Robot Science and Engineering, Northeastern University, Shenyang 110819, China*
[2]*Foshan Graduate School of Innovation, Northeastern University, Foshan 528312, China*
[3]*School of Mechanical Engineering and Automation, Northeastern University, Shenyang 110819, China*
[4]*College of Information Science and Engineering, Northeastern University, Shenyang 110819, China*
[5]*School of Mechatronics Engineering, Harbin Institute of Technology, Harbin 150001, China*

Abstract: This paper introduces a novel knee exoskeleton designed to provide assistive torque to the knee joint and facilitate postoperative rehabilitation. Drawing inspiration from the anatomy of the human knee joint, the exoskeleton incorporates a biomimetic structure that integrates the “optimal axis of rotation” with the trajectory of the instantaneous center of rotation. This design effectively mitigates the issue of kinematic misalignment in the human–machine joint, offering a more comfortable wearing experience for users. Furthermore, a highly integrated quasi-direct drive system is incorporated into the knee exoskeleton. The drive system can deliver a continuous torque of 18 N·m and a peak torque of 45 N·m to sufficiently meet the daily walking needs of patients. From a control perspective, a unified sliding mode control strategy based on iterative learning control is proposed to maintain high tracking accuracy. This strategy enables the system to achieve accurate tracking of the knee motion trajectory by continuously updating the control inputs through successive gait cycles. Experimental results demonstrate that the designed biomimetic joint mechanism effectively resolves the issue of misalignment in the human–machine joint. Furthermore, the synergistic control strategy demonstrates excellent steady-state precision and transient robustness in terms of trajectory tracking during human–exoskeleton cooperative walking.

Key words: Human–machine misalignment; Knee exoskeleton; Sliding mode control; Iterative learning control

1 Introduction

In recent years, exoskeletons have emerged as effective solutions to enhance human strength (Long et al., 2018; Aguirre-Ollinger and Yu, 2021) and restore walking ability (Dong et al., 2019; Seko et al., 2019). As the primary weight-bearing joint for lower-limb locomotion, human knee is particularly vulnerable to injury and degeneration (Zhang L et al., 2020). Consequently, with the rapid aging of the global population, the prevalence of walking impairments caused by musculoskeletal disorders, such as knee osteoarthritis, and neurological conditions like stroke, is rising continuously (Asadi Dereshgi et al., 2023). Patients suffering from knee joint dysfunction typically struggle to maintain a normal stride, often enduring reduced joint mobility and expending significantly higher metabolic energy to compensate for their impaired motor function (McCain et al., 2021). This lack of mobility not only severely restricts their independence in activities of daily living but also imposes a substantial long-term burden on healthcare systems. Therefore, the development of a compact and portable robotic knee exoskeleton holds profound clinical significance and societal value, serving to facilitate personalized home-based rehabilitation while alleviating medical care pressures.

Traditionally, most knee exoskeletons are designed with the knee joint as a simplified single hinge (Huo et al., 2019). However, this simplification fails to replicate the complex polycentric motion of the human knee, frequently resulting in kinematic misalignment between the user and the device. These misalignments can cause significant user discomfort and introduce parasitic forces that may lead to secondary joint injuries.

To address this misalignment problem, some researchers have explored various single-degree-of-freedom structures to emulate the natural knee trajectory. For example, Kim T et al. (2022) proposed a design method that approximates the actual trajectory of the knee joint by using curved guides and bearings. Hyun et al. (2017) designed a double-four-bar-based powered polycentric artificial knee joint. Kim

✉ Yi LONG, longyi@mail.neu.edu.cn
Yi LONG, https://orcid.org/0000-0003-4083-0589
CLC number: TP242; TP273

Received: Oct. 3, 2025; Revision accepted: June 3, 2026;
Crosschecked: June 10, 2026; Published online: July 28, 2026

JH et al. (2015) used a four-link mechanism to achieve multi-center motion of the real human knee joint. Wang JL et al. (2018) used a gear meshing mechanism to simulate the actual motion of the knee joint. While effective for specific anatomical profiles, these rigid structures lack versatility across diverse user populations. Celebi et al. (2013) used an underactuated structural design approach to achieve self-alignment by integrating extra passive degrees of freedom. Olinski et al. (2021) introduced two connecting rods, driven by rotating motors, to enable the four-bar mechanism to achieve a crossed configuration, thereby increasing its degrees of freedom and achieving self-alignment. Choi et al. (2017) developed a mechanism featuring several rolling cams with unique contact geometries for the knee joint to facilitate self-alignment. Lee Y et al. (2017) proposed a self-aligning joint consisting of four pulleys and two additional links. Although these self-aligning architectures successfully compensate for human–machine misalignment, they inevitably increase the overall mechanical impedance and structural complexity of the device, generating undesired interaction forces. Table 1 shows the biomimetic structure design and the overall parameter information of several knee exoskeletons. To overcome these limitations, this paper proposes a novel biomimetic structure that integrates the "optimal axis of rotation" with the trajectory of the instantaneous center of rotation.

Actuator design is another critical determinant of exoskeleton performance. Luo et al. (2017) designed a knee exoskeleton based on a series elastic actuator (SEA), which enables safe and friendly human–machine interaction. Song et al. (2023) investigated a series of elastic brakes that incorporate a crank-slider mechanism to enhance the torque effect of the actuator. Qian et al. (2023) proposed a novel nonlinear SEA (nSEA) with the characteristics of low mechanical impedance, high back drivability, and less acoustic noise. Although SEAs facilitate compliant trajectory tracking, they face numerous challenges, including limited force/torque output, low output impedance, and substantial weight and volumetric footprints. To address these issues, quasi-direct drive (QDD) actuators have emerged as a promising alternative (Chen et al., 2021; Huang et al., 2022), which can meet the high torque, high backdrivability, and high bandwidth requirements of the exoskeleton (Long and Peng, 2022). To reduce the mechanical impedance of the exoskeleton and minimize the weight of the structure, a QDD actuator is employed in this article.

The primary objective of an exoskeleton control strategy is to ensure precise trajectory tracking for the human lower limbs. However, in strongly coupled human–machine systems subject to distinct wearer characteristics and external disturbances, it is often challenging to implement model-dependent control methods, such as impedance control (Chinimilli et al., 2019) and torque control (Aguirre-Ollinger and Yu, 2021) that depend on precise system modeling. This challenge stems from the wearer's unique characteristics and external disturbances. Similarly, traditional non-model-based methods, such as proportional–integral–derivative (PID), also struggle to yield satisfactory performance in highly nonlinear environments.

Since human locomotion is inherently periodic, the iterative learning control algorithm is theoretically well-suited for such systems to achieve accurate tracking. However, the limitations of iterative learning control (ILC) are highlighted by its vulnerability to non-repetitive interference, which it handles poorly; its control accuracy degrades significantly upon encountering instantaneous dynamic variations. To overcome the inherent limitations of model dependency and vulnerability to non-repetitive disturbances, recent literature has increasingly explored advanced adaptive and learning-based strategies. For instance, Espinosa-Espejel et al. (2024) proposed an artificial neural network approach to actively estimate and compensate for external perturbations and unmodeled human–robot interactions online in real time. Similarly, model-free reinforcement learning frameworks have been developed to continuously optimize exoskeleton assistive trajectories without requiring prior dynamic models (Rv and Rakshit, 2024). Furthermore, adaptive fuzzy control schemes have been directly integrated into sliding mode control (SMC) to dynamically modulate control gains based on real-time gait errors and suppress chattering (Zhang PF and Gao, 2022). However, while these advanced machine learning paradigms exhibit exceptional environmental adaptability, their continuous weight-updating algorithms and massive exploration processes demand substantial computational resources. More importantly, they frequently suffer from delayed convergence during rapid, transient gait transitions, making real-time deployment on lightweight embedded systems highly challenging.

As a computationally efficient alternative, the SMC algorithm is relatively straightforward and exhibits exceptional robustness against external disturbances and model mismatches. Mobki et al. successfully applied multi-input decoupling (Mobki et al., 2019) and adaptive SMC (Mobki et al., 2020) to maintain absolute control across sliding surfaces and dynamically compensate for system uncertainties. Additionally, Azizi et al. (2022) used a robust nonsingular terminal sliding mode control (NTSMC) strategy to achieve high response speeds and overcome singularity in micro-electromechanical systems (MEMS) resonators. While these advanced methods perform excellently, applying their multi-input decoupling architectures, complex adaptive gain tuning, or nonsingular manifold calculations to a human–exoskeleton system characterized by high inertia and strong coupling could significantly increase hardware complexity and computational overhead.

Furthermore, while SMC is highly effective, it can also lead to a more serious jitter phenomenon (Zhang GW et al., 2022). This issue fundamentally arises from the discontinuity of the sign function

Table 1 Comparison of knee exoskeletons in the literature

Reference	Bionic structure	Weight (kg)	Peak torque (N·m)
This work	Integrating the "optimal axis of rotation" of the knee joint with the trajectory of the instantaneous center of rotation	1.6	45
Hyun et al., 2017	Double-four-bar-based powered polycentric artificial knee joint	10	
Kim JH et al., 2015	Four-bar linkage	3.5	42.9
Wang JL et al., 2018	Rolling knee joint and double-hinge mechanisms	3.2	16
Choi et al., 2017	Several rolling cams with unique contact geometries	1.23	30
Lee Y et al., 2017	Self-aligning knee joint	14.5	20

in the control law, which causes high-frequency switching of the control input and thus induces intense chattering in the system. To address this problem, Azizi (2020) replaced the conventional sign function with a tanh function, achieving a good balance between control smoothness and control accuracy. Pérez-San Lázaro et al. (2021) presented a model-free, decentralized, output-feedback, adaptive high-order SMC approach to solve the trajectory tracking problem for each degree of freedom of the exoskeleton. While this super-twisting algorithm successfully attenuates chattering and handles unknown dynamics relying solely on position feedback, its purely reactive adaptation treats periodic human gait as a series of continuous stochastic disturbances. It lacks a "memory" mechanism to exploit the rhythmic nature of walking, potentially leading to tracking lags during highly repetitive motions. Azizi et al. (2023) introduced fractional-order sliding surfaces in adaptive SMC, ensuring finite-time stability and rapid convergence of the knee joint orthosis with the desired trajectory. While this advanced fractional-order methodology provides exceptional theoretical guarantees and effective chattering suppression, its implementation inherently involves the non-local memory effect of fractional derivatives and continuous parameter estimation. Consequently, such advanced algorithms typically require high-performance hardware with substantial computational resources.

In response to attaining high tracking accuracy and strong robustness, while inherently learning periodic gait profiles without massive computational overhead, an SMC algorithm based on iterative learning control is proposed in this article. The main contribution of this study is to develop an effective solution that synergizes bio-inspired mechanical alignment with advanced periodic learning control to enhance both human–robot kinematic compatibility and dynamic tracking performance, which is summarized as follows:

1. A novel bioinspired knee joint mechanism is developed, which mathematically integrates the "optimal axis of rotation" with a dynamic pin–cam tracking profile and elastic units. This architecture fundamentally limits human–machine joint misalignment by naturally adapting to the user's instantaneous center of rotation, thereby theoretically minimizing undesired interaction forces and ensuring seamless kinematic compatibility between the human and the machine.

2. A unified iterative learning-enhanced SMC strategy is proposed, tailored for uncertain human–exoskeleton coupled dynamics. Theoretically, this framework resolves the critical trade-off between the high precision of ILC for periodic gaits and the robust disturbance rejection of SMC. By embedding the SMC algorithm as a robust learning rate within the ILC framework and substituting the discontinuous sign function with a hyperbolic tangent function, the proposed controller theoretically eliminates classical SMC chattering while maintaining exceptional tracking accuracy against non-repetitive human perturbations without requiring precise dynamic modeling.

Compared to existing methods, our proposed hardware–software synergy provides an effective and robust robotic-assisted strategy with several distinct advantages: First, unlike traditional artificial joints using four-bar linkages to realize polycentric motion or employing complex self-aligning mechanisms with multiple pulleys and links (Kim JH et al., 2015; Hyun et al., 2017; Lee Y et al., 2017), which significantly increases mechanical complexity and impedance, our bio-inspired design achieves kinematic alignment through a lightweight pin–cam architecture, maintaining high actuation transparency. Second, compared to controllers that depend on precise system modeling (Chinimilli et al., 2019; Aguirre-Ollinger and Yu, 2021) or model-free sliding mode approaches that exhibit tracking lags due to their purely reactive adaptation (Pérez-San Lázaro et al., 2021), our iterative learning (IL)-enhanced framework inherently learns the periodic gait profile to eliminate phase delay while robustly absorbing instantaneous impacts. Third, different from advanced data-driven learning paradigms like artificial neural networks and reinforcement learning (Zhang GW et al., 2022; Espinosa-Espejel et al., 2024; Rv and Rakshit, 2024) or complex fractional-order sliding mode controllers (Azizi et al., 2023), which handle unknown system dynamics at the cost of massive computational resources, continuous weight-updating, or complex parameter estimation, the proposed method provides a computationally efficient yet mathematically rigorous solution seamlessly deployable on standard embedded microcontrollers.

2 Mechanical design

2.1 Architecture of the knee exoskeleton

The architectural model of the proposed knee exoskeleton is depicted in Fig. 1. To address the critical issue of human–machine joint misalignment during exoskeleton operation, a biomimetic knee structure is designed to replicate the natural kinematics of the human knee joint. This mechanism comprises two main parts: the structural integration of the "optimal axis of rotation" and the biomimetic trajectory tracking of the instantaneous center of rotation. The central axis of the femoral condyles can be considered the "optimal axis of rotation" during knee joint rotation in the sagittal plane, enabling biomimetic motion of the human knee joint (Lewis and Lew, 1978; Churchill et al., 1998). The knee exoskeleton described in this paper employs a gear transmission system to realize the aforementioned biomimetic kinematics. In this configuration, the driving gear is positioned at the center of the knee joint line, while the driven gear is aligned with the selected "optimal axis of rotation," as illustrated in Fig. 2.

To streamline the structural design, this paper adopts the methodology proposed by Lee KM and Guo (2010) to approximate the anatomical profile of the distal femur at the knee joint as an ellipse.

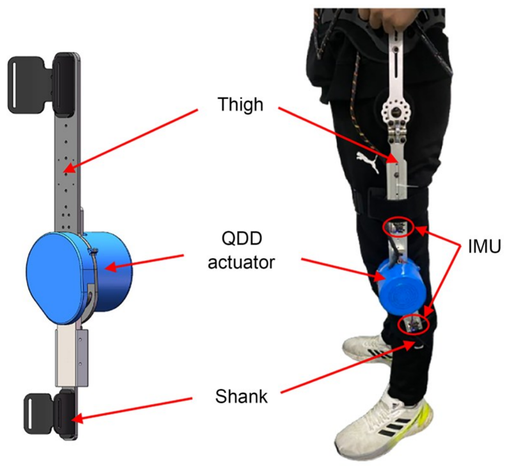

Fig. 1 Architecture of the knee exoskeleton (IMU: inertial measurement unit)

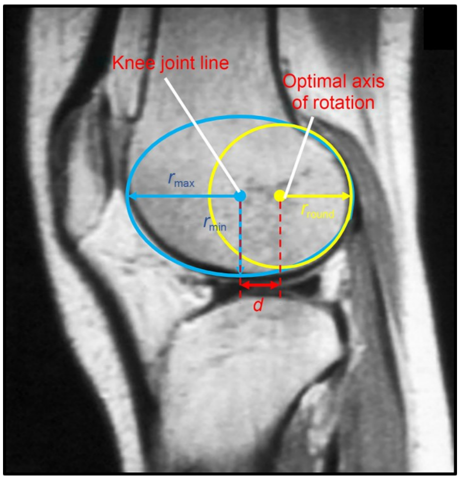

Fig. 2 Schematic of the structural principle of the "optimal axis of rotation"

Additionally, to simplify the structure, it is assumed that the center of the proposed ellipse aligns horizontally with the center of the approximating circle. The pivot offset of the knee joint can be calculated by

$$d = r_{\max} - r_{\text{round}}, \tag{1}$$

where d is the offset of the knee joint pivot, $r_{\max}$ is the length of the major axis of the ellipse, and r_{round} is the radius of the circle. From the data in the work of Lee KM and Guo (2010), we have a long oval shaft $r_{\max}$=33.6 mm and a short axis $r_{\min}$=23 mm. The radius of the approximate circle of the femoral ankle is r_{round}=21 mm, so the knee exoskeleton pivot offset d is 12.6 mm. The offset structure is realized by a gear set with a transmission ratio of 1:2, as shown in Fig. 3.

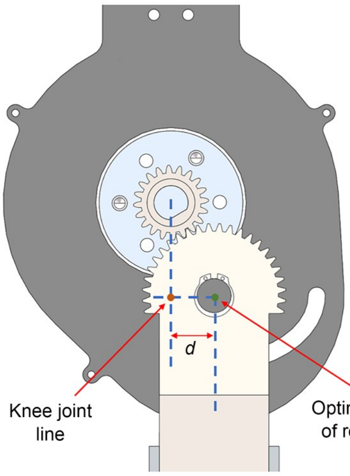

Fig. 3 The designed "optimal axis of rotation" structure

It is worth noting that during the natural flexion of the knee joint, the tibia simultaneously undergoes rotational motion around the femur and sliding motion along the contact surface. This complex articulation is facilitated by the anterior and posterior cruciate ligaments, causing the instantaneous center of rotation to trace a characteristic "J"-curve pattern. Consequently, because of the inherent anatomical variations among individuals, relying solely on the "optimal axis of rotation" can only partially mitigate the issue of misalignment between human and machine joints. It cannot fully accommodate the requirements for adapting to different levels of wear in the human body. Therefore, it is imperative to design a biomimetic mechanism capable of replicating the actual polycentric trajectory of the knee joint, built upon the foundation of the "optimal axis of rotation."

The design of the combined pin and cam structure can effectively reduce the internal joint forces and torques generated by the interaction between the human and the exoskeleton (Wang DH et al., 2014). We propose a biomimetic architecture integrating a dynamic pin–cam profile. This structural design can accommodate the motion trajectories of different human knee joints, as illustrated in Fig. 4. The cylindrical pin and the exoskeleton shank link are connected via an elastic unit. During robotic-assisted walking, if there is any residual misalignment between the mechanical joint and the biological knee, the spring within the elastic unit will deform to passively realign the trajectory of the exoskeleton with that of the human knee joint.

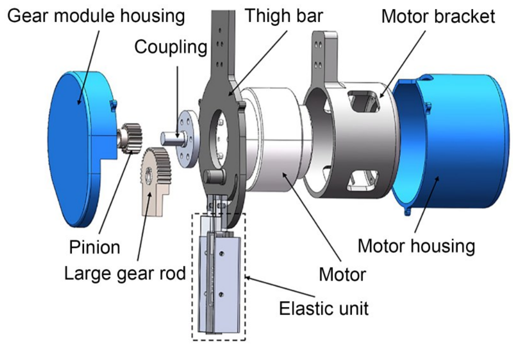

Fig. 4 The designed bionic structure of the knee exoskeleton

Importantly, because the pivot is shifted to the "optimal axis of rotation," the traditional trajectory parameters for the knee's instantaneous center of rotation may no longer be applicable. Therefore, based on the human knee joint flexion data acquired from the Vicon 3D motion capture system, by incorporating the anatomical constraints of the human knee joint, we fit a polynomial equation to serve as the design curve for the cam groove, as shown in Eq. (2):

$$y = 20 - \sqrt{-\frac{4}{9}x^2 + 400}\,,\ 0 \le x \le 30 \text{ mm}, \tag{2}$$

where x represents the horizontal displacement of the knee trajectory in the horizontal direction in the sagittal plane, and y represents the vertical displacement.

The operational principle of the proposed knee mechanism is detailed as follows: Initially, the rotational center of the exoskeleton is aligned with the "optimal axis of rotation." When the exoskeleton assists the human knee joint during flexion or extension, the motor drives the pinion through a coupling. The pinion then drives the driven gear link, which forces the cylindrical pin to traverse the contour of the cam groove, thereby rotating the human lower leg. The posterior end of the cylindrical pin is anchored to a spring. As the joint rotates, the cam's curved profile constrains the pin to translate along a linear slot. Concurrently, the exoskeleton shank link securely strapped to the human lower leg undergoes linear displacement along the same slot because of the polycentric anatomy of the human knee joint.

Because the cam profile is mathematically optimized for average biomimetic kinematics, the respective translations of both components along the linear slot are theoretically perfectly synchronized, producing zero elastic deformation in the spring. In practice, however, subject-specific variations in knee joint curvature exist among different users. This may cause discrepancies in the linear travel distances of the cylindrical pin and the shank link along the linear slot during rotation. In such cases, the spring inside the elastic unit will safely deform to absorb the differential displacement, thereby passively compensating for individual anatomical differences and ensuring high kinematic compatibility.

2.2 Design of the elastic QDD system

The mass and volumetric footprint of the actuation system directly dictate the overall portability and inertia of the knee exoskeleton. Therefore, the design of the drive system should prioritize being lightweight and integrated while ensuring the boosting effect. The peak knee joint torque during level walking for a standard healthy adult (175 cm height, 80 kg body mass) ranges from 40 N·m to 45 N·m (Long and Peng, 2022). As previously discussed, a QDD system represents an optimal solution for the stringent spatial requirements of wearable exoskeletons, owing to its compact form factor, high torque density, and exceptional backdrivability. Typically comprising a high-torque-density brushless motor paired with a low-reduction-ratio transmission, this configuration significantly minimizes mechanical impedance, a critical prerequisite for the practical deployment of transparent robotic assistance.

To create a compact and lightweight knee exoskeleton, we employ a custom, compact, and integrated QDD actuator. This actuator comprises a high-torque-density motor and a 1:36 two-stage gear reducer. The QDD actuator is capable of delivering a rated torque of 18 N·m and a peak torque of 45 N·m, while weighing just 600 g. This significantly reduces the weight of the knee exoskeleton, while providing sufficient assistive torque to meet the daily locomotive requirements of patients with knee dysfunction. Table 2 shows the detailed parameters of our knee exoskeleton.

Table 2 Specific performance of the knee exoskeleton

Parameter	Value
Weight of the QDD actuation (kg)	0.6
Movement freedom (°)	0–90
Continuous torque (N·m)	18
Peak torque (N·m)	45
Supply voltage (V)	24

During robotic-assisted locomotion, the wearer's leg and the exoskeleton constitute a tightly coupled closed-loop kinematic chain. During the rapid swing phase, abrupt directional transitions frequently generate instantaneous axial impact forces at specific joint angles, which can cause severe discomfort or potential injury to the user (Lee KM and Guo, 2010). To mitigate this, the aforementioned elastic unit is strategically incorporated at the mechanical interface between the exoskeleton shank link and the cylindrical pin structure to absorb and dissipate these instantaneous axial impacts, as illustrated in Fig. 5. The spring element we use is a customized tension/compression spring designed to achieve the same amount of displacement in both tension

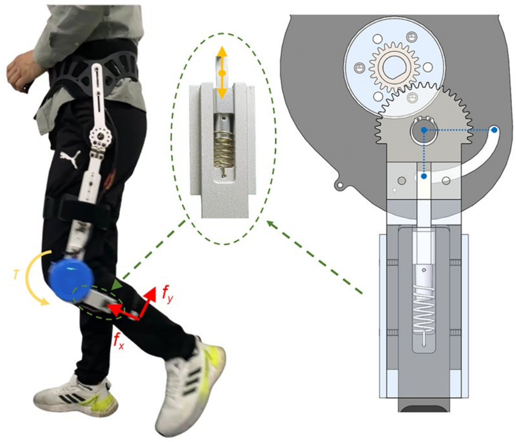

Fig. 5 Elastic unit in the real system

and compression. It has a maximum displacement of 10 mm and a stiffness coefficient of 5 N/mm.

3 Control architecture

3.1 Dynamic model of the knee exoskeleton

The knee exoskeleton and the human lower limb are rigidly coupled by straps at the thigh and calf. This configuration ensures synchronous movement between the wearer and the exoskeleton, allowing the coupled system to be simplified as a single-link model with one degree of freedom, given that knee joint flexion primarily occurs in the sagittal plane. Based on the Lagrange formulation, incorporating unmodeled dynamics such as external disturbances and friction inherent in the actual system, the dynamic model of the human–exoskeleton coupled system can be established as

$$\boldsymbol{M}(\boldsymbol{q})\ddot{\boldsymbol{q}}+\boldsymbol{C}(\boldsymbol{q},\dot{\boldsymbol{q}})\dot{\boldsymbol{q}}+\boldsymbol{G}(\boldsymbol{q})=\boldsymbol{\tau}, \tag{3}$$

$$\boldsymbol{\tau}=\boldsymbol{\tau}_{\mathrm{k}}+\boldsymbol{\tau}_{\mathrm{e}}, \tag{4}$$

$$\boldsymbol{M}\ddot{\boldsymbol{q}}=\boldsymbol{\tau}_{\mathrm{k}}+\boldsymbol{\tau}_{\mathrm{e}}-\boldsymbol{C}(\boldsymbol{q},\dot{\boldsymbol{q}})\dot{\boldsymbol{q}}-\boldsymbol{G}(\boldsymbol{q}), \tag{5}$$

where $\boldsymbol{M}(\boldsymbol{q})$ represents the inertia coefficients of the knee exoskeleton, $\boldsymbol{C}(\boldsymbol{q},\dot{\boldsymbol{q}})$ represents the centrifugal force and Coriolis coefficient matrix of the knee exoskeleton, and $\boldsymbol{G}(\boldsymbol{q})$ represents the gravity terms of the exoskeleton system. $\boldsymbol{\tau}$, $\boldsymbol{\tau}_{\mathrm{k}}$, and $\boldsymbol{\tau}_{\mathrm{e}}$ denote the total moments of the exoskeleton system, the moments generated by the exoskeleton actuator, and the external moments applied to the system respectively, which also absorb the nonlinear interaction forces from the elastic unit and soft tissues. $\boldsymbol{q}$, $\dot{\boldsymbol{q}}$, and $\ddot{\boldsymbol{q}}$ are the knee joint angle, angular velocity, and angular acceleration, respectively.

3.2 Adaptive SMC design based on ILC

As indicated by the human−machine coupled dynamic model of the knee exoskeleton, delivering precise assistive torque necessitates an accurate system representation. However, in practical scenarios, acquiring a precise dynamic model of the control system in real time is highly challenging due to inter-subject variability and unmodeled perturbations.

The proposed adaptive SMC strategy based on iterative learning control circumvents the need for precise system modeling. By synergizing the advantages of both ILC and SMC algorithms, this framework concurrently achieves high trajectory tracking accuracy and strong robustness. The high accuracy of ILC stems from its capability to progressively minimize tracking errors over successive periodic cycles. Conversely, the strong robustness of SMC arises from its inherent capacity to reject bounded disturbances during the control design phase. By integrating the SMC algorithm as the learning rate within the ILC framework, the system's robustness along the time axis is significantly enhanced. Consequently, the iterative learning process progressively attenuates tracking errors and enhances the overall tracking accuracy. The block diagram of the human–machine cooperative control strategy for the knee exoskeleton is shown in Fig. 6, where $\boldsymbol{q}_{\mathrm{d}}(t)$ and $\dot{\boldsymbol{q}}_{\mathrm{d}}(t)$ are the desired knee angle and angular velocity, respectively.

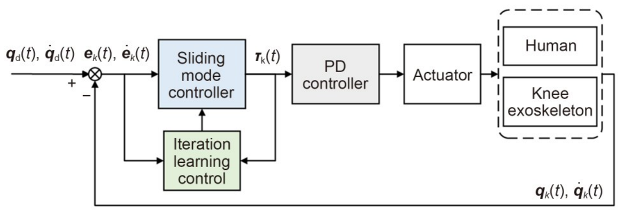

Fig. 6 Control diagram of the knee exoskeleton (PD: proportional–derivative)

As discussed above, the sliding surface is defined as

$$\boldsymbol{s}_k(t)=c\boldsymbol{e}_k(t)+\dot{\boldsymbol{e}}_k(t), \tag{6}$$

where c is a positive constant, $\boldsymbol{s}_k(t)$ denotes the sliding surface at the k^{th} iteration, $\boldsymbol{e}_k(t)=\boldsymbol{q}_{\mathrm{d}}(t)-\boldsymbol{q}(t)$ represents the k^{th} angular tracking error of the knee joint, and $\dot{\boldsymbol{e}}_k(t)=\dot{\boldsymbol{q}}_{\mathrm{d}}(t)-\dot{\boldsymbol{q}}(t)$ is the k^{th} angular velocity tracking error of the knee joint.

Differentiating both sides of Eq. (6) with respect to time yields

$$\dot{\boldsymbol{s}}_k(t)=c\dot{\boldsymbol{e}}_k(t)+\ddot{\boldsymbol{e}}_k(t)=c\dot{\boldsymbol{e}}_k+\ddot{\boldsymbol{q}}_{\mathrm{d}}(t)-\ddot{\boldsymbol{q}}(t). \tag{7}$$

Since accurately identifying dynamic parameters in practice is formidable, the dynamic properties of both the knee exoskeleton and the wearer are lumped into an unknown disturbance term. To ensure closed-loop stability, an iterative SMC strategy with an exponential reaching law is designed to formulate the output torque (Xi, 2019).

$$\boldsymbol{\tau}_{\mathrm{k}}(t)=K\boldsymbol{s}_k(t)+\hat{\varepsilon}_k(t)\operatorname{sgn}\left(\boldsymbol{s}_k(t)\right), \tag{8}$$

$$\hat{\varepsilon}_k(t)=\hat{\varepsilon}_{k-1}(t)+\sigma\left\|\boldsymbol{s}_k(t)\right\|, \tag{9}$$

where K and σ are positive constants. ε represents the unknown constant upper bound of the lumped system dynamics, which effectively acts as the ideal reaching rate required to compensate for these uncertainties. $\hat{\varepsilon}_k(t)$ serves as the adaptive estimator of ε at the k^{th} iteration, satisfying $\hat{\varepsilon}_0(t)=0$. The parameter σ acts as the iterative learning rate within the adaptation law, governing how effectively the estimator $\hat{\varepsilon}_k(t)$ converges to the ideal bound ε across successive gait cycles. $\operatorname{sgn}(x)$ denotes the sign function.

Due to the inherent discontinuous nature of SMC and the influence of system inertia and hysteresis, classical SMC inevitably suffers from the chattering phenomenon. In this paper, the sign function in the ideal sliding mode is replaced by a hyperbolic tangent function to achieve a smooth control output:

$$\tanh(s)=\frac{\mathrm{e}^{s}-\mathrm{e}^{-s}}{\mathrm{e}^{s}+\mathrm{e}^{-s}}. \tag{10}$$

In summary, the control law of the knee exoskeleton can be obtained as

$$\boldsymbol{\tau}_{\mathrm{k}}(t)=K\boldsymbol{s}_k(t)+\hat{\varepsilon}_k(t)\tanh\left(\boldsymbol{s}_k(t)\right). \tag{11}$$

The stability and convergence of the proposed knee exoskeleton control strategy are analyzed as follows:

Lemma 1 $\boldsymbol{M}\in\mathbb{R}^{n\times n}$ is a positive definite and bounded symmetric array.

Lemma 2 $\dot{\boldsymbol{M}}-2\boldsymbol{C}$ is a skew-symmetric matrix and satisfies $\boldsymbol{x}^{\mathrm{T}}(\dot{\boldsymbol{M}}-2\boldsymbol{C})\boldsymbol{x}=0, \forall\boldsymbol{x}\in\mathbb{R}^{n}$.

Typically, the lemmas are satisfied for dynamic models of knee exoskeletons that satisfy the form of Eq. (3).

Remark 1 It should be explicitly noted that the skew-symmetry property stated in Lemma 2 conventionally applies to purely rigid-body Lagrangian systems. In our modeling of the human–exoskeleton coupled system (Eq. (3)), the human lower limb and the exoskeleton segments are approximated as a lumped rigid-body link. This approximation is physically justified by the tight fastening between the exoskeleton and the human limb, which allows them to be treated as tightly bound equivalent rigid units in the nominal dynamics (Xiao et al., 2026). The restoring forces originating from the physical elastic unit and the human–machine interface are mathematically decoupled from the kinetic energy matrices and are instead treated as external interaction torques $\boldsymbol{\tau}_{\mathrm{e}}$. Consequently, the inertial matrix $\boldsymbol{M}(\boldsymbol{q})$ and the Coriolis matrix $\boldsymbol{C}(\boldsymbol{q},\dot{\boldsymbol{q}})$ are formulated solely based on the lumped rigid inertial parameters, preserving the strict skew-symmetry of the nominal model. Furthermore, any minor violations of this rigid-body assumption—arising from human soft-tissue deformations or unmodeled elastic nonlinearities in practical scenarios—are consolidated into the bounded disturbance term. The inherent robustness of the proposed SMC framework is specifically designed to reject these very deviations, ensuring global stability despite potential local violations of the idealized model.

Furthermore, the following assumptions are established for the dynamic equations of the knee exoskeleton system:

Assumption 1 The desired trajectory of the knee exoskeleton $\boldsymbol{q}_{\mathrm{d}}(t)$, its first-order derivatives $\dot{\boldsymbol{q}}_{\mathrm{d}}(t)$, and second-order derivatives $\ddot{\boldsymbol{q}}_{\mathrm{d}}(t)$ are bounded, and the uncertainty and perturbation terms are also bounded.

Assumption 2 The iterative process satisfies the initial state repeatability, which means $\boldsymbol{q}_{\mathrm{d}}(0)-\boldsymbol{q}(0)=\boldsymbol{0}$ and $\dot{\boldsymbol{q}}_{\mathrm{d}}(0)-\dot{\boldsymbol{q}}(0)=\boldsymbol{0}$.

1. Definition of the Lyapunov function and boundedness proof

In this paper, the Lyapunov energy function is constructed as

$$E_k(t)=\frac{1}{2}\boldsymbol{s}_k^{\mathrm{T}}\boldsymbol{M}\boldsymbol{s}_k+\frac{1}{2\sigma}\int_0^t\tilde{\varepsilon}_k^2(\tau)\,\mathrm{d}\tau, \tag{12}$$

where $\tilde{\varepsilon}_k(t)=\varepsilon(t)-\hat{\varepsilon}_k(t)$. To facilitate the derivation of the formula, let

$$V_k(t)=\frac{1}{2}\boldsymbol{s}_k^{\mathrm{T}}\boldsymbol{M}\boldsymbol{s}_k. \tag{13}$$

By Lemma 2, we have

$$\dot{V}_k(t)=\boldsymbol{s}_k^{\mathrm{T}}\boldsymbol{M}\dot{\boldsymbol{s}}_k+\frac{1}{2}\boldsymbol{s}_k^{\mathrm{T}}\dot{\boldsymbol{M}}\boldsymbol{s}_k=\boldsymbol{s}_k^{\mathrm{T}}\left(\boldsymbol{M}\dot{\boldsymbol{s}}_k+\boldsymbol{C}\boldsymbol{s}_k\right). \tag{14}$$

From Eqs. (5) and (7), we can obtain

$$\boldsymbol{M}\dot{\boldsymbol{s}}_k=\boldsymbol{M}\left(c\dot{\boldsymbol{e}}_k+\ddot{\boldsymbol{q}}_{\mathrm{d}}\right)+\boldsymbol{C}\dot{\boldsymbol{q}}+\boldsymbol{G}-\boldsymbol{\tau}_{\mathrm{k}}-\boldsymbol{\tau}_{\mathrm{e}}. \tag{15}$$

We add and subtract $\boldsymbol{C}\boldsymbol{s}_k$ on the right side. Expanding $\boldsymbol{C}\boldsymbol{s}_k$ yields

$$\boldsymbol{M}\dot{\boldsymbol{s}}_k=-\boldsymbol{C}\boldsymbol{s}_k-\boldsymbol{\tau}_{\mathrm{k}}+\boldsymbol{H}_k, \tag{16}$$

where $\boldsymbol{H}_k=\boldsymbol{M}\left(c\dot{\boldsymbol{e}}_k+\ddot{\boldsymbol{q}}_{\mathrm{d}}\right)+\boldsymbol{C}\left(c\boldsymbol{e}_k+\dot{\boldsymbol{q}}_{\mathrm{d}}\right)+\boldsymbol{G}-\boldsymbol{\tau}_{\mathrm{e}}$ represents the unknown lumped system dynamics. Given the physical constraints of the human–exoskeleton system and the smoothness of reference trajectories, $\boldsymbol{H}_k$ is assumed to be bounded such that $\|\boldsymbol{H}_k\|\le\varepsilon$. We can obtain $\dot{V}_k=\boldsymbol{s}_k^{\mathrm{T}}\left(\boldsymbol{H}_k-\boldsymbol{\tau}_{\mathrm{k}}\right)$.

Considering the control input in Eq. (11), it can be concluded that

$$\begin{aligned}\dot{V}_k&=\boldsymbol{s}_k^{\mathrm{T}}\left(\boldsymbol{H}_k-K\boldsymbol{s}_k-\hat{\varepsilon}_k\tanh\left(\boldsymbol{s}_k\right)\right)\\&\le\left(\varepsilon-\hat{\varepsilon}_k\right)\|\boldsymbol{s}_k\|-K\boldsymbol{s}_k^{\mathrm{T}}\boldsymbol{s}_k\\&=\tilde{\varepsilon}_k\|\boldsymbol{s}_k\|-K\boldsymbol{s}_k^{\mathrm{T}}\boldsymbol{s}_k.\end{aligned} \tag{17}$$

Integrating both sides of the equation yields

$$\begin{aligned}V_k(t)&\le V_k(0)+\int_0^t\left(\tilde{\varepsilon}_k\|\boldsymbol{s}_k\|-K\boldsymbol{s}_k^{\mathrm{T}}\boldsymbol{s}_k\right)\mathrm{d}\tau\\&\le\int_0^t\left(\tilde{\varepsilon}_k\|\boldsymbol{s}_k\|-K\boldsymbol{s}_k^{\mathrm{T}}\boldsymbol{s}_k\right)\mathrm{d}\tau.\end{aligned} \tag{18}$$

Calculate the difference of the Lyapunov energy function for successive iterations:

$$\begin{aligned}\Delta E_k&=E_k-E_{k-1}\\&=V_k-V_{k-1}-\frac{1}{2\sigma}\int_0^t\left[\left(\tilde{\varepsilon}_k-\tilde{\varepsilon}_{k-1}\right)^2-2\tilde{\varepsilon}_k\left(\tilde{\varepsilon}_k-\tilde{\varepsilon}_{k-1}\right)\right]\mathrm{d}\tau.\end{aligned} \tag{19}$$

Substituting inequality (18) into Eq. (19), it can be concluded that

$$\begin{aligned}\Delta E_k&\le\int_0^t\left(\tilde{\varepsilon}_k\|\boldsymbol{s}_k\|-K\boldsymbol{s}_k^{\mathrm{T}}\boldsymbol{s}_k\right)\mathrm{d}\tau-V_{k-1}-\frac{\sigma}{2}\int_0^t\|\boldsymbol{s}_k\|^2\mathrm{d}\tau-\int_0^t\tilde{\varepsilon}_k\|\boldsymbol{s}_k\|\mathrm{d}\tau\\&\le-V_{k-1}-\int_0^t\left(K\boldsymbol{s}_k^{\mathrm{T}}\boldsymbol{s}_k+\frac{\sigma}{2}\|\boldsymbol{s}_k\|^2\right)\mathrm{d}\tau\le0.\end{aligned} \tag{20}$$

From the above inequality, E_k is a nonincreasing sequence. Then, it is sufficient to show that $E_0(t)$ is bounded to prove the boundedness of $E_k(t)$. Therefore, when k=0, it can be obtained from Eq. (12) that

$$\begin{aligned}E_0(t)&=\frac{1}{2}\boldsymbol{s}_0^{\mathrm{T}}\boldsymbol{M}\boldsymbol{s}_0+\frac{1}{2\sigma}\int_0^t\tilde{\varepsilon}_0^2(\tau)\mathrm{d}\tau\\&=V_0(t)+\frac{1}{2\sigma}\int_0^t\tilde{\varepsilon}_0^2(\tau)\mathrm{d}\tau.\end{aligned} \tag{21}$$

Differentiating Eq. (21) with respect to time yields

$$\dot{E}_0=\dot{V}_0(t)+\frac{1}{2\sigma}\tilde{\varepsilon}_0^2. \tag{22}$$

When k=0, we can obtain

$$\dot{V}_0\le\tilde{\varepsilon}_0\|\boldsymbol{s}_0\|-K\boldsymbol{s}_0^{\mathrm{T}}\boldsymbol{s}_0. \tag{23}$$

Substituting inequality (23) into Eq. (22) yields

$$\begin{aligned}\dot{E}_0&\le\tilde{\varepsilon}_0\|\boldsymbol{s}_0\|-K\boldsymbol{s}_0^{\mathrm{T}}\boldsymbol{s}_0+\frac{1}{2\sigma}\tilde{\varepsilon}_0^2\\&=\varepsilon\|\boldsymbol{s}_0\|+\frac{1}{2\sigma}\varepsilon^2-K\boldsymbol{s}_0^{\mathrm{T}}\boldsymbol{s}_0\le N.\end{aligned} \tag{24}$$

Integrating both sides of the inequality with respect to t, we have

$$\begin{aligned}E_0(t)&\le\int_0^tN\mathrm{d}\tau=Nt+E_0(0)\\&\le NT+E_0(0).\end{aligned} \tag{25}$$

Since $E_0(0)$ and N are finite, it can be concluded that $E_0(t)$ is continuous and bounded on the interval $[0,T]$; $E_k(t)$ is bounded on the interval $[0,T]$.

2. Proof of the convergence of the sliding mode function

It is possible to rewrite E_k in the following form:

$$E_k=E_0+\sum_{i=1}^{k}\Delta E_i. \tag{26}$$

Then it can be deduced from inequality (20) that

$$E_k\le E_0-\sum_{i=1}^{k}V_{i-1}\le E_0-\frac{1}{2}\sum_{i=1}^{k}\boldsymbol{s}_{i-1}^{\mathrm{T}}\boldsymbol{M}\boldsymbol{s}_{i-1}, \tag{27}$$

$$\frac{1}{2}\sum_{i=1}^{k}\boldsymbol{s}_{i-1}^{\mathrm{T}}\boldsymbol{M}\boldsymbol{s}_{i-1}\le E_0-E_k\le E_0. \tag{28}$$

Since E_0 is bounded, the following limits hold on the interval $[0,T]$:

$$\lim_{k\to\infty}\boldsymbol{s}_{k-1}(t)=\boldsymbol{0},\ \forall t\in[0,T], \tag{29}$$

$$\lim_{k\to\infty}\boldsymbol{s}_k(t)=\boldsymbol{0},\ \forall t\in[0,T]. \tag{30}$$

4 Experiments and results

4.1 Participants

To evaluate the performance of the proposed knee exoskeleton, experiments were conducted with three healthy male volunteers (26±3 years old, 175±10 cm, 76±9 kg). To ensure safety and familiarization, a test engineer trained the volunteers the day before the formal experiments, detailing the operational protocols, essential functionalities, and necessary safety precautions. Subsequently, the volunteers engaged in free walking practice while wearing the device to eliminate potential discomfort caused by improper donning and to mitigate possible risks.

4.2 Experiments on human–machine misalignment compensation

The purpose of the human–machine joint alignment experiments is to validate the effectiveness of the knee exoskeleton's biomimetic structure. These experiments were conducted with the participant wearing the exoskeleton in an unpowered, completely passive state, as depicted in Fig. 7. The experiments used a Vicon 3D motion capture system to acquire real-time positional information of marker points located on the lower limbs of the human body. The experiments were conducted with the participant on a treadmill, moving at a speed of 3 km/h.

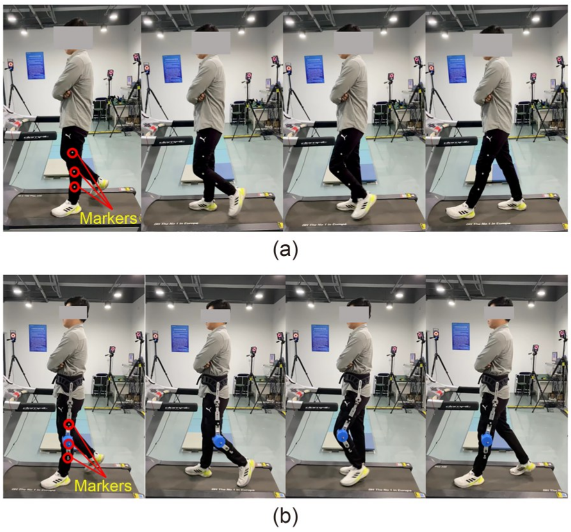

Fig. 7 Human–machine misalignment compensation experiments: (a) human knee joint motion trajectory capturing experiments; (b) knee exoskeleton joint trajectory capturing experiments

Furthermore, to quantitatively compare the kinematic trajectory of the exoskeleton knee with the instantaneous center of rotation of the human knee, a distal reference point on the lower leg was established. Specifically, we selected the calf binding position as this reference point. The anatomical distance from the marker at the knee joint to the marker at the calf binding was measured to be 185 mm. Strict experimental controls were implemented to ensure that the marker locations remained identical across both conditions: with and without the exoskeleton.

In the joint alignment experiments, the sagittal plane of the human knee joint was calibrated to align with the *YOZ* plane of the 3D motion capture system. The *YOZ* coordinate data of the marker points within the same plane can effectively demonstrate the trajectory characteristics of the knee joint. Therefore, these coplanar data were selected for trajectory fitting. Since the 3D spatial data obtained from the optical motion capture system are relative to the absolute global coordinate system, a coordinate transformation in the *YOZ* plane was necessary. This transformation calculated the relative coordinates of the calf marker points in relation to the knee marker points. The data within this relative coordinate plane were then used to represent the kinematic trajectory of the knee joint. To mitigate potential errors in data acquisition, trajectory data for both the human knee and the exoskeleton were averaged over 10 continuous gait cycles. Subsequently, the final averaged trajectories were compared and analyzed. The experimental results from three different subjects are presented in Fig. 8.

Fig. 8 illustrates the kinematic consistency between the exoskeleton knee trajectories and the actual human knee trajectories for the three participants. The red solid line represents the actual trajectory of the human knee, while the blue dashed line represents the trajectory of the exoskeleton knee. As shown in the figure, the mean square error of the experimental data of the three subjects was 0.41, 0.73, and 0.81 mm^2, respectively. These results demonstrate that the designed biomimetic knee structure generally aligns well with that of the human knee joint. However, during the initial leg swing phase, the transient trajectories of subject 1 and subject 3 while wearing the exoskeleton display slight deviations during knee flexion compared to the actual human kinematics, with a maximum deviation of 1.25 mm. The trajectory curves of subject 2, while generally consistent, still exhibit some minor deviations during the flexion process. These variations may be attributed to mechanical tolerances, such as the difference in width between the cam groove and the cam roller, which is essential for ensuring smooth movement. Additionally, potential wear in the cams and slots can lead to increased clearances. These factors may cause the calf link to experience minor drops due to gravity.

The captured trajectories of the knee joints for all three subjects exhibit a characteristic "J"-shaped curve. This is highly consistent with the anatomical descriptions of the instantaneous center of rotation trajectory of the human knee joint. Therefore, it can be concluded that the captured in vivo instantaneous trajectories of the human knee joints and the exoskeleton mechanisms are both biomechanically reasonable and reliable.

By comparing the actual knee trajectories of the three participants, it can also be observed that the trajectories of the instantaneous center of rotation vary across individuals due to anatomical differences. However, overall, they exhibit similar trajectory shapes. The proposed

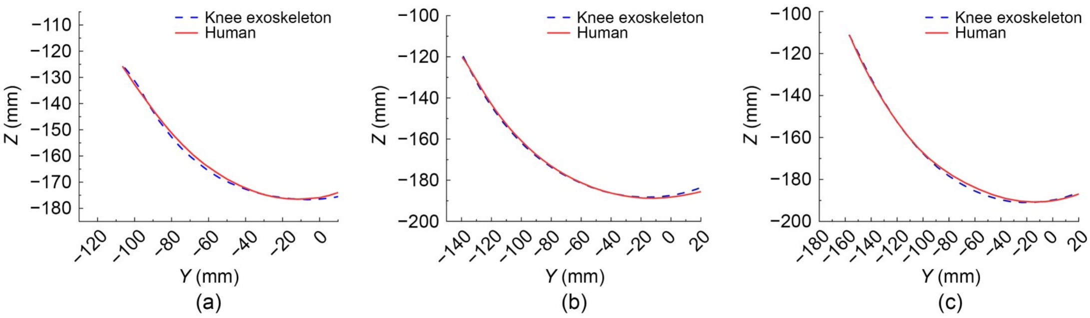

Fig. 8 Comparison of human–exoskeleton joint trajectories: (a) subject 1; (b) subject 2; (c) subject 3

biomimetic structure of the knee joint can adapt to these individual variations among different wearers, achieving real-time alignment between the human leg and the exoskeleton knee joint. This alignment is fundamentally based on the specific polycentric trajectory characteristics of the human knee joint.

4.3 Experiments on wearing the knee exoskeleton

When the exoskeleton assists the wearer in rehabilitation training or daily walking, the control system must exhibit minimal tracking error, high robustness, and fast response capabilities. To validate the performance of the designed control strategy, experiments were conducted to evaluate the exoskeleton's ability to assist the participant in tracking target trajectories. For the real-time execution of the exoskeleton, the proposed IL-enhanced SMC and the baseline PID algorithms were programmed in C language. The embedded control software was developed within the Keil Microcontroller Development Kit (MDK) integrated development environment (IDE) and deployed onto an STM32 microcontroller. The control loop was executed at a deterministic sampling frequency of 100 Hz. Joint angle measurements were acquired using an absolute magnetic encoder (MT6825) with an 18-bit resolution and a miniature IMU (LPMS-CURS3) with an angular resolution of <0.01°. To clearly demonstrate the trajectory tracking performance of the knee exoskeleton, the wearer's baseline knee motion trajectories were first collected at five different walking speeds: 1, 1.5, 2, 2.5, and 3 km/h. These collected data were then processed via MATLAB for trajectory smoothing and fitting to train an offline trajectory generator. The speed-specific gaits produced by this generator were subsequently used as the desired reference trajectories for the knee joint during the treadmill walking experiments. The experimental process is shown in Fig. 9.

The results of the knee trajectory tracking experiments are depicted in Fig. 10. The red solid line represents the intended trajectory of the knee joint, while the blue dashed line represents the actual motion trajectory during robotic assistance. It is evident that the

Fig. 9 Experiments on wearing the knee exoskeleton on the treadmill

proposed control strategy effectively assists the wearer's knee in following the desired trajectory across all five movement speeds. Figs. 10a and 10b demonstrate that at relatively low speeds, the exoskeleton can assist the wearer in completing the overall gait phase smoothly. However, as the walking speed increases to the mid-speed transition phase shown in Figs. 10c and 10d, it is evident that the tracking performance exhibits more pronounced oscillations along the sliding surface. This is particularly noticeable when entering the stance phase and during the transition between stance and swing. These increased oscillations may be attributed to the higher gait variability and more fluctuating dynamic interactions at these transitional speeds, ultimately leading to larger dynamic tracking deviations. In Fig. 10e, the knee exoskeleton assists the wearer in achieving stable and smooth movement again. This recovery in tracking performance is thanks to the highly periodic nature of the high walking speed, which allows the iterative learning algorithm to effectively anticipate and track the trajectory. Overall, the control strategy of the designed knee exoskeleton enables more accurate trajectory tracking, aiding the wearer in recovering their normal walking ability in a stable and smooth manner.

The green curve in Fig. 10 represents the error curve of knee trajectory tracking. It can be observed that at lower walking speeds (Figs. 10a and 10b), the range of knee angle tracking error is approximately (−5°, 5°), and the overall trajectory error remains relatively stable. During the mid-speed transition phase (Figs. 10c and 10d), the tracking error of the angle increases due to higher gait variability,

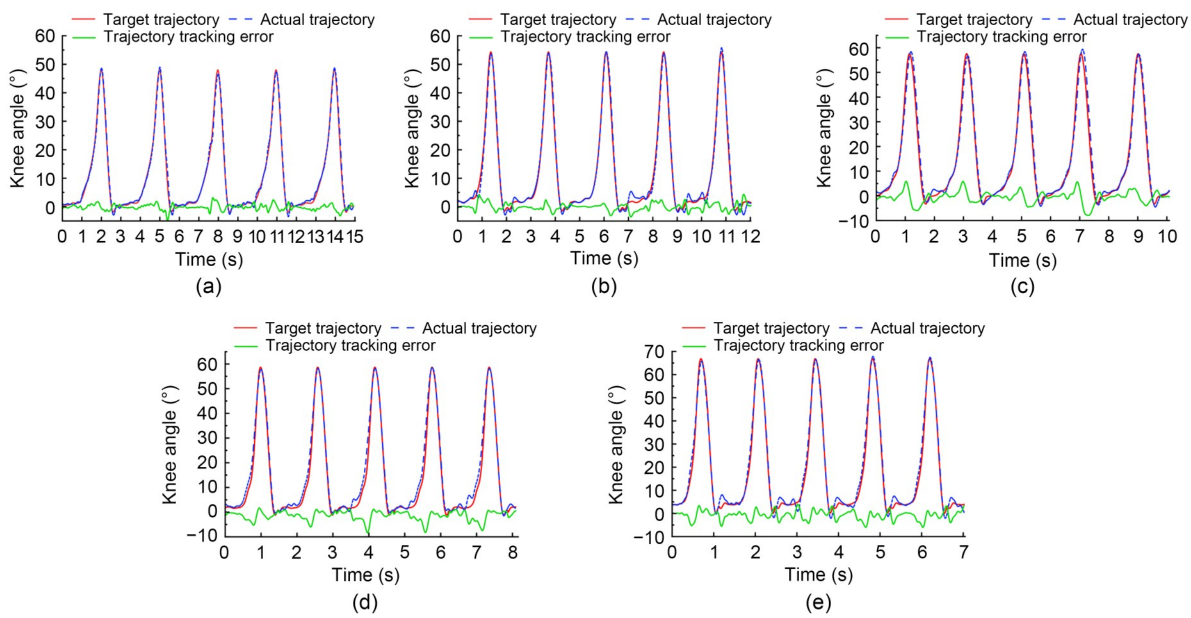

Fig. 10 Human–exoskeleton trajectory tracking results of the proposed IL-enhanced SMC at different speeds: (a) 1 km/h; (b) 1.5 km/h; (c) 2 km/h; (d) 2.5 km/h; (e) 3 km/h

falling within a broader range of approximately (−9°, 6°), and the error fluctuation becomes more significant. However, at the highly periodic high-walking speed (Fig. 10e), the error fluctuation is effectively mitigated and narrowed. It can be observed that the control strategy ensures smooth assistance of the knee exoskeleton to the human body while walking at different speeds. Furthermore, the system stably converges to the desired trajectory.

To robustly evaluate the control performance, Fig. 11 and Table 3 quantitatively compare the proposed IL-enhanced SMC with a baseline PID controller based on iterative learning. From the results presented in Table 3, the proposed controller demonstrates highly precise trajectory tracking, yielding a root mean square error (RMSE) as low as 1.05° at 1 km/h. It is noteworthy that the tracking error experiences a peak during the mid-speed transition phase, reaching an RMSE of 2.51° at 2 km/h and a maximum error of 8.37° at 2.5 km/h. This phenomenon aligns with human biomechanics, as mid-speed locomotion often exhibits higher gait variability, more fluctuating dynamic interactions, and less stable periodicity. However, as the walking speed increases to 3 km/h, the wearer transitions into a highly stable and strictly periodic fast-walking gait. Because the feedforward mechanism of the ILC algorithm fundamentally excels at learning and anticipating highly repetitive periodic signals, the tracking accuracy is effectively restored at 3 km/h, reducing the RMSE to 2.16° and bounding the maximum error to 5.98°. In contrast, the baseline PID controller based on iterative learning struggles significantly to adapt to these dynamic variations across the speed spectrum, with its RMSE escalating from 1.65° to 5.40°, and its maximum error surging to an unacceptable 21.70° at higher speeds. This degradation in the baseline controller is primarily attributed to the increased impact forces and unmodeled dynamic fluctuations during the transition between the stance and swing phases at elevated speeds. The proposed IL-enhanced SMC successfully suppresses these non-repetitive disturbances through the robust reaching law of the sliding surface.

Table 3 Comparison of tracking errors under different control methods and walking speeds

Control method	Error type	Error value (°)				
		1 km/h	1.5 km/h	2 km/h	2.5 km/h	3 km/h
Proposed IL-enhanced SMC	RMSE	1.05	1.34	2.51	2.46	2.16
	Maximum error	4.93	4.32	7.92	8.37	5.98
PID based on iterative learning	RMSE	1.65	2.32	4.38	4.14	5.40
	Maximum error	5.04	6.54	17.77	21.70	20.14

Furthermore, to highlight the superiority of the proposed IL-enhanced SMC architecture, its performance is compared with those of well-known and recent control strategies applied to exoskeleton systems. Classical control algorithms fundamentally struggle with the highly nonlinear and time-varying coupled dynamics of human–exoskeleton interaction. For instance, despite extensive parameter tuning, optimal PID controllers in recent exoskeleton studies exhibit tracking limitations, yielding an RMSE of approximately 4.65° under dynamic load conditions (Pathak et al., 2026). Model-free approaches, such as active disturbance rejection control (ADRC), address these unmodeled dynamics but typically suffer from response lag. A recent study on a lower-knee exoskeleton demonstrated that conventional linear ADRC yielded an RMSE of approximately 3.1° (0.0541 rad) under load disturbances (Alawad et al., 2025). While the transfer-function active disturbance rejection control (TFADRC) improves steady-state precision, its purely reactive nature still struggles to eliminate phase lag during high-speed transient phases.

Alternatively, conventional SMC provides robustness against parameter uncertainties but inherently suffers from severe chattering. Mitigating these fundamental SMC defects generally necessitates computationally heavy architectures, such as high-order super-twisting algorithms coupled with nonlinear disturbance observers (Raheem et al., 2026).

The proposed IL-enhanced SMC architecture resolves these theoretical and practical limitations by directly exploiting the periodic nature of human locomotion. Unlike reactive controllers, the ILC feedforward mechanism continuously learns and anticipates the repetitive joint profile, effectively neutralizing the phase lag typical

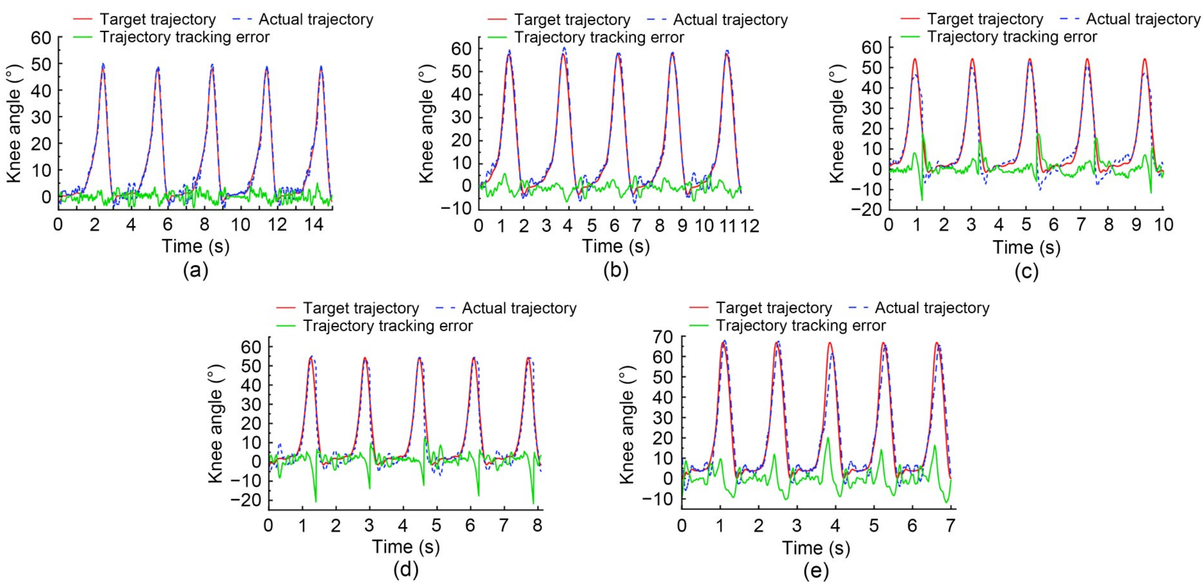

Fig. 11 Human–exoskeleton trajectory tracking results of PID control based on iterative learning at different speeds: (a) 1 km/h; (b) 1.5 km/h; (c) 2 km/h; (d) 2.5 km/h; (e) 3 km/h

of ADRC and PID controllers. Simultaneously, adaptive SMC mitigates non-repetitive instantaneous impacts without inducing high-frequency chattering or requiring complex, computationally heavy observer dynamics. By strictly bounding the maximum dynamic RMSE within 2.51° across the entire speed spectrum and robustly suppressing transient errors, the proposed framework demonstrates superior steady-state tracking precision, transient robustness, and computational efficiency over classical algorithms for dynamic gait assistance.

5 Conclusions

In this paper, a novel robotic-assisted knee exoskeleton is designed to assist patients with knee dysfunction in restoring their walking capabilities. To fundamentally address human–machine kinematic misalignment, we propose a biomimetic structural design for the knee joint. Guided by human anatomy, the pivot axis is shifted from the conventional knee joint line to the anatomical "optimal axis of rotation," which significantly improves joint ergonomics. In addition, we develop a dynamic pin–cam mechanism that can seamlessly adapt to various human knee kinematic trajectories. To enhance the driving performance while maintaining a compact and lightweight form factor, a custom elastic QDD actuator is integrated into the exoskeleton.

To achieve robust human–machine cooperative control, a unified iterative learning-enhanced SMC strategy is designed, and the global stability of the system is rigorously analyzed. Finally, the kinematic compatibility of the designed biomimetic structure is effectively validated using a 3D motion capture system to assess human–machine joint alignment. Furthermore, the trajectory tracking efficacy of the designed control strategy is tested on a treadmill. The experimental results demonstrate that the proposed biomimetic structure effectively eliminates misalignment in the exoskeleton's joint components. Simultaneously, the synergistic control strategy enables the wearer to achieve highly accurate trajectory tracking, thereby validating its promising potential to assist in restoring normal walking ability.

6 Future research recommendations

While the present study demonstrates the feasibility and effectiveness of the proposed knee exoskeleton and its synergistic control strategy, several key avenues remain to be explored in our future work, which are outlined as follows:

1. Mechanism optimization and biomechanical alignment. Future research will investigate the optimal offset distance of the "optimal axis of rotation" and refine the design of the cam curves based on this structure to more accurately align with the individual trajectories of the human knee joint.

2. Hardware integration and lightweight design. We will perform rigorous performance tests on the QDD actuator to explore further possibilities for achieving a lighter and more compact knee exoskeleton design.

3. Environmental adaptation and personalized control. Future work will extend the framework to handle complex environments (e.g., slopes and stairs) and explicitly address gait cycle variability (such as changes in stride length or cadence). Furthermore, we will explore "human-in-the-loop" optimization, where control parameters are automatically tuned in real time (e.g., via gradient-free optimization algorithms) to match user-specific gait characteristics, thereby enhancing comfort and personalized rehabilitative efficiency.

4. Long-term clinical studies and safety mechanisms. Longitudinal clinical trials will be conducted to evaluate the rehabilitative efficacy for specific patient populations. Simultaneously, we will focus on enhancing hardware-level fail-safe mechanisms and sophisticated fault-detection algorithms to ensure the system's reliability and safety in complex real-world scenarios.

Acknowledgments

This work was supported by the Fundamental Research Funds for the Central Universities (No. N25GFY006) and the Natural Science Foundation of Liaoning Province (No. 2025-MS-040).

Author contributions

Yi LONG and Ning CHEN designed the bionic structure of the knee exoskeleton. Ning CHEN and Zhibin CAI co-designed the controller. Hexiao GUO and Yutian CHI processed and organized the experimental data. Wei DONG provided guidance on experimental validation methods and result interpretation. Ning CHEN drafted and revised the paper. All the authors read and approved the final paper.

Conflict of interest

All the authors declare that they have no conflict of interest.

The participants have all signed an informed consent prior to their participation. The experimental protocol was approved by the Institutional Review Board at Northeastern University. None of the volunteers had prior experience with a robotic exoskeleton.

Data availability

The data that support the findings of this study are available from the corresponding author upon reasonable request.

Declaration on the use of generative AI tools

During the preparation of this work, the authors did not use any generative AI tools. All content was independently created, written, and revised by the authors, who take full responsibility for the integrity and accuracy of the paper.

References

Aguirre-Ollinger G, Yu HY, 2021. Lower-limb exoskeleton with variable-structure series elastic actuators: phase-synchronized force control for gait asymmetry correction. *IEEE Trans Robot*, 37(3):763-779. https://doi.org/10.1109/TRO.2020.3034017

Alawad NA, Humaidi AJ, Muslim MM, 2025. Modified ADRC for position lower-knee exoskeleton system: rehabilitation case. *Int Rev Appl Sci Eng*, 16(2):314-323. https://doi.org/10.1556/1848.2024.00922

Asadi Dereshgi H, Göse E, Demir D, et al., 2023. Restoring mobility and independence: evaluating the impact of knee exoskeletons in real-world scenarios. *J Smart Syst Res*, 4(1):61-71. https://doi.org/10.58769/joinssr.1308638

Azizi A, 2020. A case study on designing a sliding mode controller to stabilize the stochastic effect of noise on mechanical structures: residential buildings equipped with ATMD. *Complexity*, 2020:9321928. https://doi.org/10.1155/2020/9321928

Azizi A, Mobki H, Ouakad HM, et al., 2022. Applied mechatronics: on mitigating disturbance effects in MEMS resonators using robust nonsingular terminal sliding mode controllers. *Machines*, 10(1):34. https://doi.org/10.3390/machines10010034

Azizi A, Naderi Soorki M, Vedadi Moghaddam T, et al., 2023. A new fractional-order adaptive sliding-mode approach for fast finite-time control of human knee joint orthosis with unknown dynamic. *Mathematics*, 11(21):4511. https://doi.org/10.3390/math11214511

Celebi B, Yalcin M, Patoglu V, 2013. AssistOn-Knee: a self-aligning knee exoskeleton. Proc IEEE/RSJ Int Conf on Intelligent Robots and Systems, p.996-1002.

https://doi.org/10.1109/IROS.2013.6696472
Chen SY, Stevenson DT, Yu SY, et al., 2021. Wearable knee assistive devices for kneeling tasks in construction. *IEEE/ASME Trans Mechatron*, 26(4):1989-1996. https://doi.org/10.1109/TMECH.2021.3081367
Chinimilli PT, Qiao Z, Rezayat Sorkhabadi SM, et al., 2019. Automatic virtual impedance adaptation of a knee exoskeleton for personalized walking assistance. *Robot Auton Syst*, 114:66-76. https://doi.org/10.1016/j.robot.2019.01.013
Choi B, Lee Y, Kim YJ, et al., 2017. Development of adjustable knee joint for walking assistance devices. Proc IEEE/RSJ Int Conf on Intelligent Robots and Systems, p.1790-1797. https://doi.org/10.1109/IROS.2017.8205993
Churchill DL, Incavo SJ, Johnson CC, et al., 1998. The transepicondylar axis approximates the optimal flexion axis of the knee. *Clin Orthop Relat Res*, 356:111-118. https://doi.org/10.1097/00003086-199811000-00016
Dong WC, Liu CC, Zhang Q, et al., 2019. Design and evaluation of an active ankle exoskeleton in gait assistance. Proc IEEE/ASME Int Conf on Advanced Intelligent Mechatronics, p.318-322. https://doi.org/10.1109/AIM.2019.8868740
Espinosa-Espejel KI, Rosales-Luengas Y, Salazar S, et al., 2024. Active disturbance rejection control via neural networks for a lower-limb exoskeleton. *Sensors*, 24(20):6546. https://doi.org/10.3390/s24206546
Huang TH, Zhang SN, Yu SY, et al., 2022. Modeling and stiffness-based continuous torque control of lightweight quasi-direct-drive knee exoskeletons for versatile walking assistance. *IEEE Trans Robot*, 38(3):1442-1459. https://doi.org/10.1109/TRO.2022.3170287
Huo WG, Mohammed S, Amirat Y, 2019. Impedance reduction control of a knee joint human-exoskeleton system. *IEEE Trans Contr Syst Technol*, 27(6):2541-2556. https://doi.org/10.1109/TCST.2018.2865768
Hyun DJ, Park H, Ha T, et al., 2017. Biomechanical design of an agile, electricity-powered lower-limb exoskeleton for weight-bearing assistance. *Robot Auton Syst*, 95:181-195. https://doi.org/10.1016/j.robot.2017.06.010
Kim JH, Shim M, Ahn DH, et al., 2015. Design of a knee exoskeleton using foot pressure and knee torque sensors. *Int J Adv Robot Syst*, 12(8):112. https://doi.org/10.5772/60782
Kim T, Jeong M, Kong K, 2022. Bioinspired knee joint of a lower-limb exoskeleton for misalignment reduction. *IEEE/ASME Trans Mechatron*, 27(3):1223-1232. https://doi.org/10.1109/TMECH.2021.3099815
Lee KM, Guo JJ, 2010. Kinematic and dynamic analysis of an anatomically based knee joint. *J Biomech*, 43(7):1231-1236. https://doi.org/10.1016/j.jbiomech.2010.02.001
Lee Y, Kim YJ, Lee J, et al., 2017. Biomechanical design of a novel flexible exoskeleton for lower extremities. *IEEE/ASME Trans Mechatron*, 22(5):2058-2069. https://doi.org/10.1109/TMECH.2017.2718999
Lewis JL, Lew WD, 1978. A method for locating an optimal "fixed" axis of rotation for the human knee joint. *J Biomech Eng*, 100(4):187-193. https://doi.org/10.1115/1.3426209
Long Y, Peng YJ, 2022. Design and control of a quasi-direct drive actuated knee exoskeleton. *J Bion Eng*, 19(3):678-687. https://doi.org/10.1007/s42235-022-00168-2
Long Y, Du ZJ, Wang WD, et al., 2018. Human motion intent learning based motion assistance control for a wearable exoskeleton. *Robot Comput-Integr Manuf*, 49: 317-327. https://doi.org/10.1016/j.rcim.2017.08.007
Luo YH, Wang C, Wang Z, et al., 2017. Design and control for a compliant knee exoskeleton. Proc IEEE Int Conf on Information and Automation, p.282-287. https://doi.org/10.1109/ICInfA.2017.8078920
McCain EM, Libera TL, Berno ME, et al., 2021. Isolating the energetic and mechanical consequences of imposed reductions in ankle and knee flexion during gait. *J Neuroeng Rehabil*, 18(1):21. https://doi.org/10.1186/s12984-021-00812-8
Mobki H, Jalilirad M, Vatankhah Moradi M, et al., 2019. Multi input versus single input sliding mode for closed-loop control of capacitive micro structures. *SN Appl Sci*, 1(7):676. https://doi.org/10.1007/s42452-019-0728-5
Mobki H, Sabegh AM, Azizi A, et al., 2020. On the implementation of adaptive sliding mode robust controller in the stabilization of electrically actuated micro-tunable capacitor. *Microsyst Technol*, 26(12):3903-3916. https://doi.org/10.1007/s00542-020-04882-x
Olinski M, Gronowicz A, Ceccarelli M, 2021. Development and characterisation of a controllable adjustable knee joint mechanism. *Mech Mach Theory*, 155:104101. https://doi.org/10.1016/j.mechmachtheory.2020.104101
Pathak LK, Mittal H, Gopaliya SM, et al., 2026. Design, modeling, and control of a knee exoskeleton for underwater load assistance. 4th Int Conf on Sustainable Technologies and Advances in Automation, Aerospace and Robotics, Article 01007. https://doi.org/10.1051/epjconf/202635501007
Pérez-San Lázaro R, Salgado I, Chairez I, 2021. Adaptive sliding-mode controller of a lower limb mobile exoskeleton for active rehabilitation. *ISA Trans*, 109:218-228. https://doi.org/10.1016/j.isatra.2020.10.008
Qian YP, Han SS, Wang YN, et al., 2023. Toward improving actuation transparency and safety of a hip exoskeleton with a novel nonlinear series elastic actuator. *IEEE/ASME Trans Mechatron*, 28(1):417-428. https://doi.org/10.1109/TMECH.2022.3201255
Raheem FA, Hasan AF, Flaieh EH, et al., 2026. A nonlinear disturbance observer-based super-twisting sliding mode controller for a knee-assisted exoskeleton robot. *Automation*, 7(1):23. https://doi.org/10.3390/automation7010023
Rv M, Rakshit S, 2024. Deep reinforcement learning based control of lower limb exoskeleton. Proc Int Joint Conf on Neural Networks, p.1-6. https://doi.org/10.1109/IJCNN60899.2024.10651057
Seko S, Matthew RP, Riemer R, 2019. Passive knee assistance affects whole-body biomechanics during sit-to-stand. Proc 41st Annual Int Conf of the IEEE Engineering in Medicine and Biology Society, p.4440-4444. https://doi.org/10.1109/EMBC.2019.8856477
Song JY, Zhu AB, Tu Y, et al., 2023. Novel design and control of a crank-slider series elastic actuated knee exoskeleton for compliant human–robot interaction. *IEEE/ASME Trans Mechatron*, 28(1):531-542. https://doi.org/10.1109/TMECH.2022.3204921
Wang DH, Lee KM, Guo JJ, et al., 2014. Adaptive knee joint exoskeleton based on biological geometries. *IEEE/ASME Trans Mechatron*, 19(4):1268-1278. https://doi.org/10.1109/TMECH.2013.2278207
Wang JL, Li X, Huang TH, et al., 2018. Comfort-centered design of a lightweight and backdrivable knee exoskeleton. *IEEE Robot Autom Lett*, 3(4):4265-4272. https://doi.org/10.1109/LRA.2018.2864352
Xi WQ, 2019. Research on Construction and Control of Coordinated Multi-Robots System. PhD Dissertation, Nanjing University of Aeronautics and Astronautics, Nanjing, China (in Chinese). https://doi.org/10.27239/d.cnki.gnhhu.2019.002021
Xiao HR, Ran T, Jin AF, 2026. Dynamic modelling and control strategy analysis of a lower-limb exoskeleton. *Sensors*, 26(7):2124. https://doi.org/10.3390/s26072124
Zhang GW, Wang J, Yang P, et al., 2022. A learning control scheme for upper-limb exoskeleton via adaptive sliding mode technique. *Mechatronics*, 86:102832. https://doi.org/10.1016/j.mechatronics.2022.102832
Zhang L, Liu G, Han B, et al., 2020. Assistive devices of human knee joint: a review. *Robot Auton Syst*, 125:103394. https://doi.org/10.1016/j.robot.2019.103394
Zhang PF, Gao XS, 2022. Fuzzy adaptive sliding mode control of lower limb exoskeleton rehabilitation robot. *Proc Rom Acad Ser A*, 23(4):383-391.